applied sciences

MDPI

Article

Evaluation of Spring Stiffness of Resilience Pads for Booted Sleeper Track System Using a Pressure Sensor

Jung-Youl Choi, Jee-Seung Chung, Dae-Hui Ahn * and Jae-Min Han

Department of Construction Engineering, Dongyang University, No. 145 Dongyangdae-ro, Punggi-eup, Yeongju-si 36040, Republic of Korea
* Correspondence: ahndh@dyu.ac.kr; Tel.: +82-54-630-1092

Abstract: To date, the spring stiffness of resilience pads was mostly evaluated based on conventional (site measurement and laboratory tests) methods. Most studies in the past analyzed the effects of the deterioration of resilience pads on track damage. To examine the deterioration of resilience pads, evaluations were conducted based on laboratory tests using site measurements and samples were collected from the site, or based on loading tests using special equipment. such as TSS. However, no methodology was proposed to prove the theoretical equations of Zimmermann which compute the reaction force at the rail support point. Hence, this study aimed to prove that the reaction force increased if spring stiffness at the rail support point increased; this was achieved by using a pressure sensor according to the theoretical equations of Zimmermann. Furthermore, we aimed to propose a method to evaluate the spring stiffness of resilience pads to predict the extent of deterioration of the pads based on the increase in the pressure measured by a pressure sensor.

Keywords: pressure sensor; spring stiffness; resilience pad; booted sleeper track system; evaluation method

check for updates

Citation: Choi, J.-Y.; Chung, J.-S.; Ahn, D.-H.; Han, J.-M. Evaluation of Spring Stiffness of Resilience Pads for Booted Sleeper Track System Using a Pressure Sensor. *Appl. Sci.* **2023**, *13*, 4002. https://doi.org/10.3390/app13064002

Academic Editor: Diogo Ribeiro

Received: 16 February 2023
Revised: 16 March 2023
Accepted: 20 March 2023
Published: 21 March 2023

Copyright: © 2023 by the authors. Licensee MDPI, Basel, Switzerland. This article is an open access article distributed under the terms and conditions of the Creative Commons Attribution (CC BY) license (https://creativecommons.org/licenses/by/4.0/).

1. Introduction

In recent years, the market size of urban railway maintenance (damage assessment, diagnosis, repair, and reinforcement) expanded. In South Korea, related laws (enforcement ordinances) were implemented for the systematic inspection, diagnosis, and performance evaluation of track facilities, and diagnoses and performance evaluations were performed on a regular basis. However, few studies were conducted on methods that evaluate elastic materials, which are key components of concrete tracks. For the elastic-pad performance evaluation based on current standards, on-site measurement is performed for trains in operation or the static spring stiffness is measured in a laboratory by collecting samples from the field. On-site measurement is a technique used to estimate the spring stiffness of elastic materials by measuring the dynamic wheel load and vertical displacement of the rail during train passage and calculating the track support stiffness. In the laboratory tests used for on-site samples, a static spring stiffness test is conducted in a laboratory on elastic materials collected from tracks in operation through nighttime construction. However, this method cannot fully reflect actual field conditions, and nighttime track construction is required for sampling [1,2].

Most domestic urban railways comprise concrete tracks, and the track support stiffness that directly affects the performance of concrete tracks is determined by the spring stiffness of the elastic pads. Therefore, deteriorated elastic materials may increase shock and vibration, compromise riding comfort, cause complaints, and deteriorate other track components, including rails. Elastic materials may lose their functions over time owing to deterioration; thus, maintenance, such as replacement, must be performed in a timely manner through status assessment [1,2].

Figure 1 shows the conventional evaluation techniques that are proposed in this study [1,2].

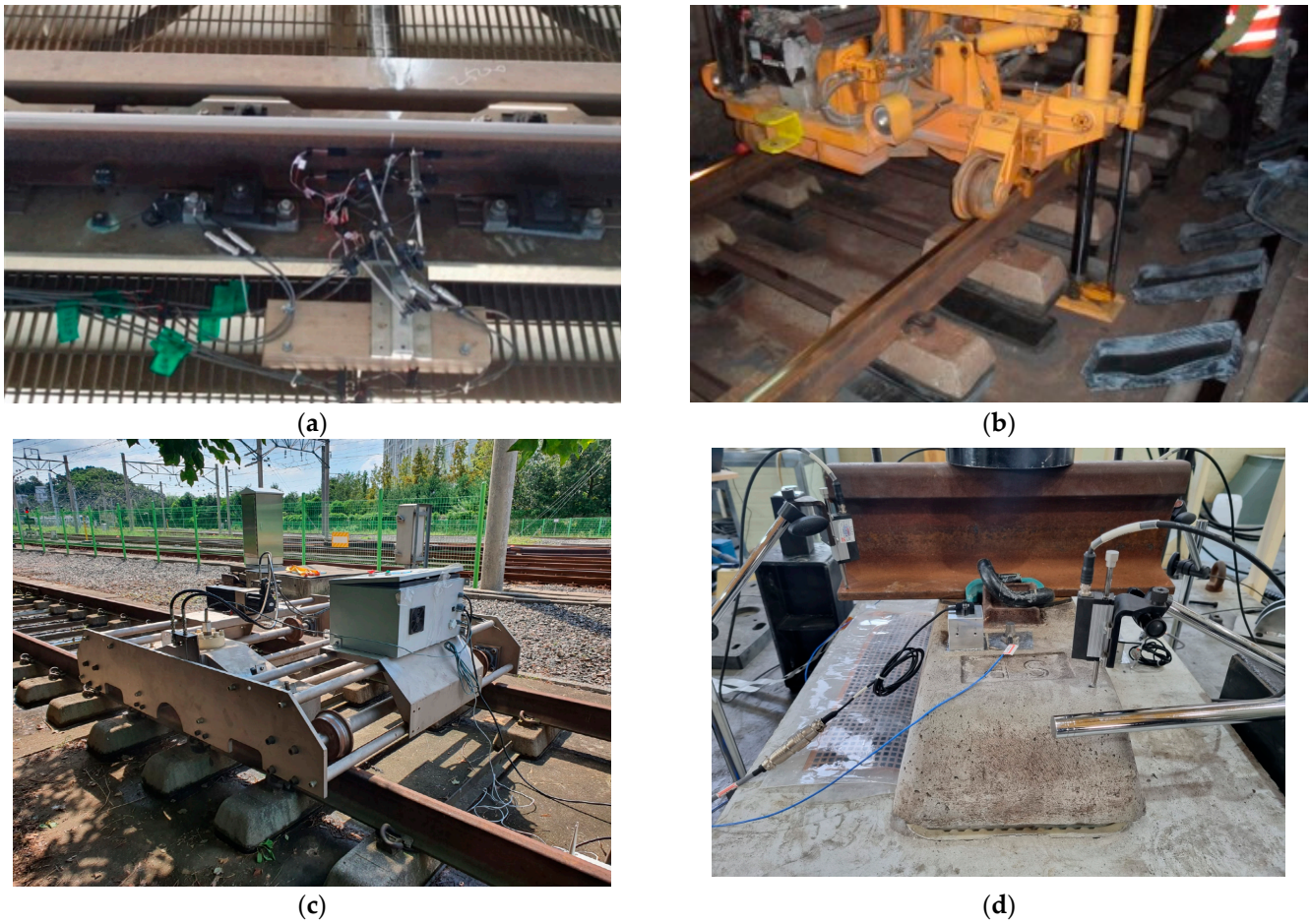


Figure 1. Track performance evaluation techniques: (**a**) on-site measurement technique (based on strain gauges); (**b**) laboratory test through sampling; (**c**) TSS equipment evaluation technique; and (**d**) evaluation technique using a pressure sensor.

Thus far, track performance was mostly evaluated using the techniques shown in Figure 1a,b. For on-site measurement on tracks in operation, wheel load and lateral pressure sensors as well as displacement meters are installed at the site during the nighttime power-outage period, as shown in Figure 1a. In addition, track performance must be evaluated under the actual train load during the daytime train-operation period [1,2]. In the laboratory test conducted on samples, a vertical stiffness test was conducted on a laboratory scale by collecting elastic pads from the site, as shown in Figure 1b. For the test, collecting elastic pads at the site by dismantling rail fastenings and lifting sleepers is necessary. In addition, the spring stiffness of the elastic pads must be evaluated through a vertical stiffness test on the collected elastic pads. Figure 1c shows the recently developed test equipment used to evaluate the performance of concrete tracks. The TSS equipment can apply a train load and evaluate track performance by calculating the spring stiffness of elastic pads immediately after measurement [1]. However, the performance-evaluation techniques shown in Figure 1a–c cannot directly evaluate resilience pads, which are the main evaluation target. That is, they indirectly evaluate the track support stiffness through the vertical displacement of the rail under the train load and predict the spring stiffness of elastic pads by calculating the rail support spring stiffness [1,2].

Li et al. used Monte Carlo simulations (MCS), which are based on statistical analyses, to analyze the correlation between the deformation behavior and the shape and size of aggregates. The analyzed results showed that aggregate behavior was affected significantly by the elongation index (EI) distribution, and was less affected by the excitation frequency and flatness index (FI) distribution [3]. Fu et al. conducted an analysis by setting the

support conditions at the bottom of the sleeper according to the surrounding environment (gravel loss due to flooding, etc.) as a variable to evaluate safety in the case in which a partial concrete sleep replacement method was applied for a gravel track laid with wooden sleepers. In addition, they proposed a technique to predict the sleep support conditions using an acceleration sensor installed on the rail and then, determined the train speed limit [4]. Navaratnarajah et al. analyzed the sleep-gravel track interface for the shear behavior of a gravel track when there are various types of sleepers. The analyzed results showed that both commercial and recycled USP significantly improved the shear resistance at the contact surface between sleeper and gravel track, and that particle decomposition decreased compared with the contact surface between the concrete and wooden sleeper [5]. Previous studies mostly used a strain gauge to measure the wheel load, and LVDT were used to measure the vertical displacements of the rail and sleeper. Spring stiffness at the rail support point was estimated based on the measured results.

However, in this study, a pressure sensor was directly installed on the elastic pad to evaluate the pressure under the train load, as shown in Figure 1d. Pressure was used to determine the reaction force at the rail support point, and the changes in spring stiffness at the rail support point could be found. The change in elastic pad spring stiffness is a factor that directly affects the track support performance and is highly correlated with pressure. Therefore, this study presents a system that can evaluate this change.

The booted sleeper track system (STEDEF) was selected as the research target among various types of concrete tracks. The STEDEF is a track system that is embedded in the roadbed. It is a structure in which concrete sleepers are separated from the concrete bed, and highly elastic resilience pads are installed inside the rubber boots. This structure minimizes the transmission of the vibration and shock caused by the train load to the track structure [6].

This study proposes a technique to evaluate the change in the spring stiffness of resilience pads by measuring the pressure generated at the bottom of a concrete sleeper using a pressure measurement sensor, which is defined as a pressure sensor. Figure 2 shows the pressure sensor installation location.

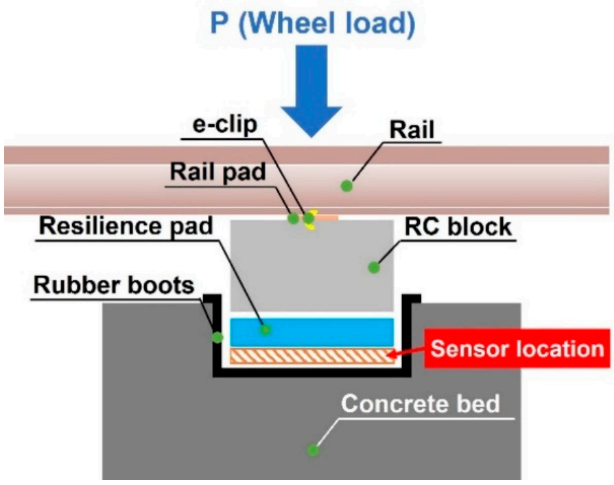


Figure 2. Pressure sensor location (STEDEF).

In this study, a pressure sensor was installed between the resilience pad and rubber boots of the STEDEF to measure the generated pressure, as shown in Figure 2. The existing track-performance evaluation method was performed based on the change in track support stiffness, which is an indicator of support performance under the application of the train load and a factor that can directly affect tracks and vehicles. It is also a major factor that affects the static and dynamic behavior of tracks and is important for evaluation [2,6].

The analysis of previous studies revealed that the STEDEF is a structure that involves changes in track support stiffness and pressure at the bottom of the sleeper depending on

the uplift and settlement. A decrease in track support stiffness can be evaluated under the settlement condition; thus, the pressure at the bottom of the sleeper may decrease. Under the uplift condition, the pressure may increase owing to an increase in track support stiffness, which can be evaluated. Therefore, uplift and settlement sections can be evaluated using the change in pressure at the bottom of the sleeper as well as the increase/decrease in track support stiffness.

Track support stiffness can be evaluated through the theoretical equations of Zimmermann [2]. The equations used for calculating the deflection of rails, which are continuously supported infinite beams, and rail support spring stiffness are as follows [2]:

$$w(x) = \frac{QL^3}{8EI} e^{-\left(\frac{x}{L}\right)} \left(cos\frac{x}{L} + sin\frac{x}{L}\right), \tag{1}$$

$$M(x) = \frac{QL}{4} e^{-\left(\frac{x}{L}\right)} \left(cos\frac{x}{L} - sin\frac{x}{L}\right), \tag{2}$$

$$F(x) = \frac{Qa}{2L} e^{-\left(\frac{x}{L}\right)} \left(cos\frac{x}{L} + sin\frac{x}{L}\right), \tag{3}$$

where EI is the bending stiffness of the rail, Q is the vertical force, $w(x)$ is the rail displacement at position x, $M(x)$ is the rail moment at position x, and $F(x)$ is the pressure load on the sleeper at position x. The characteristics length L is as follows [2]:

$$L = \sqrt[4]{\frac{4EI}{k_c}} = \sqrt[4]{\frac{4EI\,a}{k_s}}, \tag{4}$$

where L is the characteristic length of track, k_c is the track support stiffness, k_s is the rail support spring stiffness, and a is the sleeper distance. The equation used to calculate the k_s value of the STEDEF is given by Equation (5) [2]. Figure 3 shows the spring model [6].

$$k_s = \frac{1}{\frac{1}{k_1} + \frac{1}{k_2} + \frac{1}{k_3}}, \tag{5}$$

where k_1 is the spring stiffness of the rail pad, k_2 is the stiffness of the resilience pad, and k_3 is the spring stiffness of the rubber boots [6]. Rail support spring stiffness is directly affected by the spring stiffness of the track components. Thus, an increase in the spring stiffness of the elastic pad may decrease the rail characteristic length or increase the reaction force at the rail support point or the pressure transmitted to the bottom of the sleeper. However, measuring the pressure at the bottom of the sleeper is difficult for track types, such as the STEDEF. Thus far, track support stiffness and rail support spring stiffness were evaluated for the STEDEF using the wheel load and the vertical displacement of rail converted through strain gauges and low vibration displacement transducers (LVDTs). The spring stiffness of elastic pads is calculated by installing strain sensors, such as LVDT, at the site, and by calculating track support stiffness using the measured wheel load and displacement. The calculated track support stiffness was used to compute the spring stiffness of the rail support point. The spring stiffnesses of the elastic pads were also calculated.

In this study, a pressure sensor was installed at the bottom of the resilience pad, which directly affects the rail support spring stiffness, to measure the pressure according to the load. In addition, the validity of the pressure sensor was verified through laboratory tests and numerical analysis. Based on the research results, a technique is proposed to evaluate the spring stiffness of resilience pads via a pressure measurement at the bottom of the sleeper.

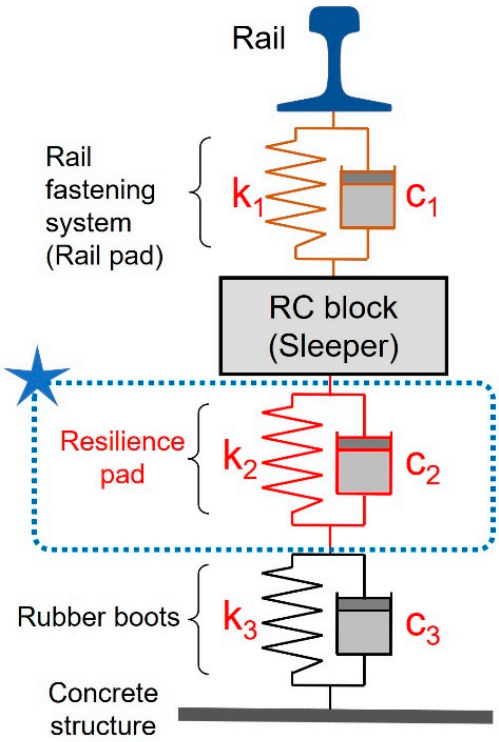


Figure 3. Booted sleeper track system spring model.

2. Materials and Methods

For the pressure sensor used in this study, the magnitude of its electrical resistance changes depending on the applied force or pressure. The physical definition of pressure is the load divided by the cross-sectional area, and it changes depending on the area under the same load. Pressure sensors are generally thin, with a thickness of less than 0.5 mm, light, and strong against impact. They are typically used to measure the pressure distribution on robot hands, human gloves, solid surfaces, and medical appliances [7–12]. In this study, a pressure sensor was applied to the railway (track) field. Figure 4 shows the measurement principle of the pressure sensor that was used.

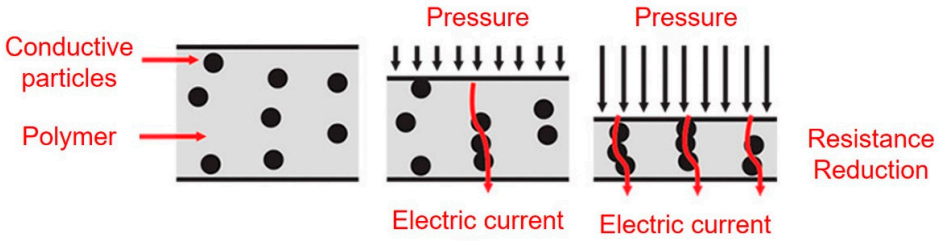


Figure 4. Pressure sensor measurement principle.

In the pressure sensor, conductive particles move closer to each other inside the polymer when pressure (load) is applied from the outside. When a load is applied on the pressure sensor, the resistance value between the particles is produced as an analog signal. This signal needs to be converted into a digital signal to derive the applied load value from the measurement system. For the pressure-sensor saturation criterion applied in this study, the maximum pressure measurement was set when the signal value through an analog-to-digital converter (ADC) reached a maximum of 255 (8 bits). Because the pressure sensor measures the load based on the resistance value between the particles, a resistance-value deviation may exist owing to fabrication errors. After the pressure sensor was fabricated, it was calibrated by measuring the ADC signal according to the applied load set by the user. Figure 5 shows the signal measurement test according to the set load.

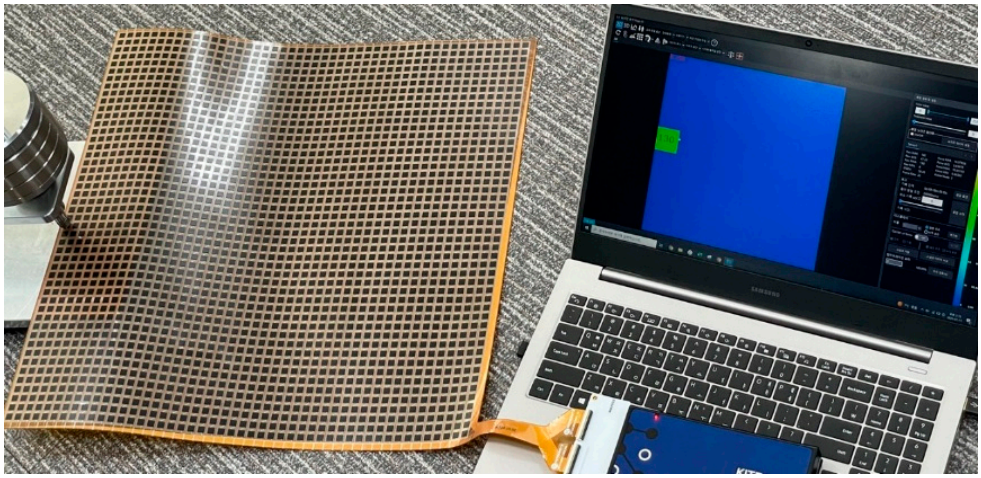


Figure 5. Pressure-sensor calibration.

As shown in Figure 5, the ADC signal value was measured for each load set by the user. Figure 6 shows an example of measurement results.

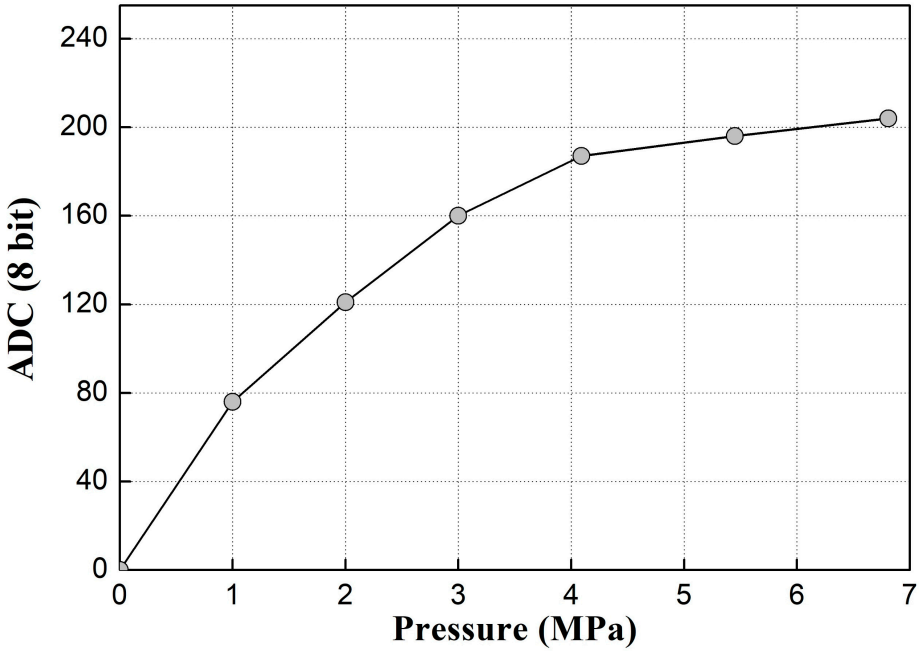


Figure 6. ADC measurement results according to the load (example).

For the pressure sensor, digital signal values were measured according to the load (pressure) set by the user, as shown in Figure 6. Using the pressure-sensor calibration, the magnitude of the load was measured when a load was applied, as shown in Figure 6.

Figure 7 and Table 1 show the specifications of the pressure sensor used in this study and an example of visualization software for the measurement results.

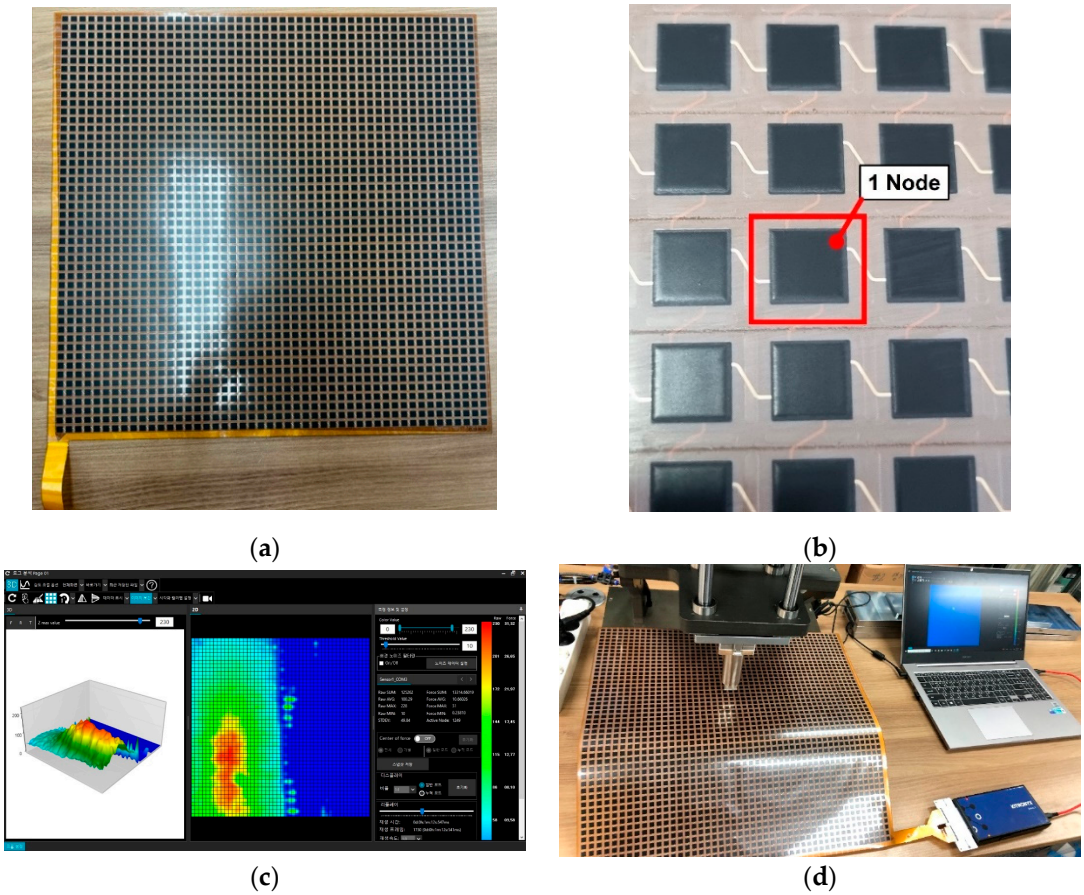


Figure 7. Pressure sensor and visualization software: (**a**) pressure sensor; (**b**) pressure sensor node (detail); (**c**) example of pressure sensor measurement software; (**d**) pressure sensor measurement system.

Table 1. Main specifications of the pressure sensor.

Sensor size	442 × 442 mm	Sensing area size	431 × 431 mm
Cell size	5 × 5 mm	Pitch (=center to center)	9 mm/9 mm
Temperature range	−20–60 °C	Number of rows	48
Number of columns	48	Number of nodes	2304 (48 × 48)

This study examined the validity of the pressure sensor. The maximum pressure detected, accuracy, measurement speed, and measurement area were verified as validity criteria. The maximum pressure detected was determined by the saturation of the ADC value owing to the pressure increase. The ADC produced a measurement of 187 under a pressure of 4.09 MPa, 196 under 5.45 MPa, and 204 under 6.81 MPa. Thus, the observations proved that the pressure sensor could measure more than 6.81 MPa.

The pressure-sensor accuracy was determined using the error of the values measured when the set pressure was applied two or more times. When 1.36 MPa was applied and re-applied, the measurement was 1.38 MPa, and the error rate was observed to be less than 1.5%. For the measurement speed, measurements were performed under the application of pressure, and the sampling rate was then determined from the number of datapoints recorded per second. The pressure sensor used in this study had a total of 48 × 48 (2304) nodes, and it was observed that 32 datapoints were recorded per second per node. Therefore, the sampling rate was determined to be 73,728 (=2304 × 32) Hz.

To determine the measurement area of the pressure sensor, the length and width of the sensing area of the sample were measured to be 428 × 428 mm. Therefore, the error from the sensing area considered for the design was regarded as insignificant.

As shown in Figure 6c, the system applied in this study can display the measurement results of the pressure sensor in two-dimensional (2D) and three-dimensional (3D) graphs. The performance of the system was verified at a laboratory scale before its application to an actual STEDEF site for the development of a technique for evaluating the aging (deterioration) of resilience pads and changes in track boundary conditions by measuring the pressure at the bottom of the sleeper via a pressure sensor.

3. Laboratory Tests

3.1. Overview

In this study, static and dynamic loading tests were conducted on the STEDEF assembly. The static loading test was conducted within the rail fastening system (KRS-TR-0014-15R) standard of the Korean railway standards [13]. The dynamic loading test was also conducted to verify the performance of the pressure sensor. Figure 8 shows the installation of the STEDEF and pressure sensor for laboratory tests.

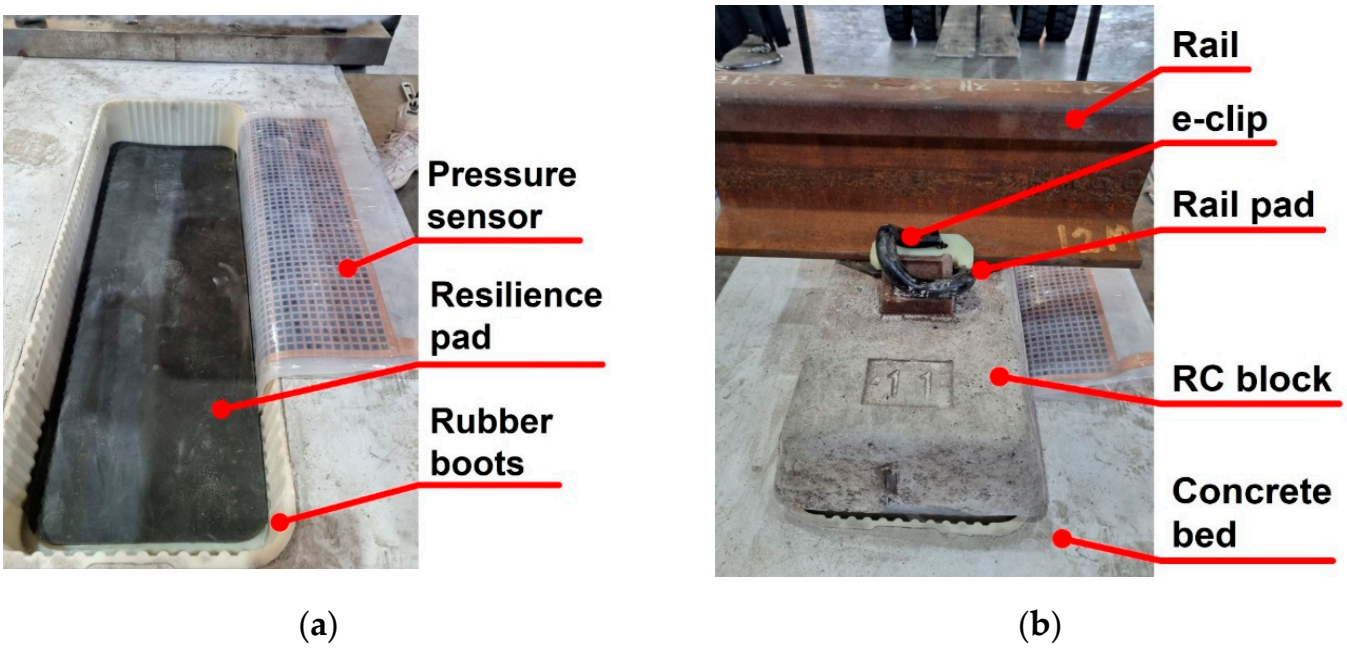


Figure 8. STEDEF and pressure sensor: (**a**) pressure sensor installed; (**b**) STEDEF assembly.

In this study, the pressure sensor was installed between the STEDEF components, as shown in Figure 8. In the laboratory tests, the vertical displacements of the rail and sleeper as well as the pressure at the bottom of the sleeper were measured. The vertical displacements were used to calculate the spring stiffness of the resilience pad. Figure 9 shows the measurement items for the laboratory tests.

The vertical displacements of the rail and sleeper were measured using LVDTs. A sufficient sampling rate (1.0 kHz) was set to prevent the distortion and loss of measurement data signals as much as possible and remove the signals of noise components.

The pressure sensor was inserted between the resilience pad and rubber boots to measure the pressure under the application of a load. The pressure-sensor measurement data were simultaneously obtained from a total of 2304 nodes by setting the maximum sampling rate to 30 Hz for each node. In the case of the dynamic loading test, the maximum excitation frequency was 4 Hz, and the pressure-sensor sampling rate was judged to be appropriate.

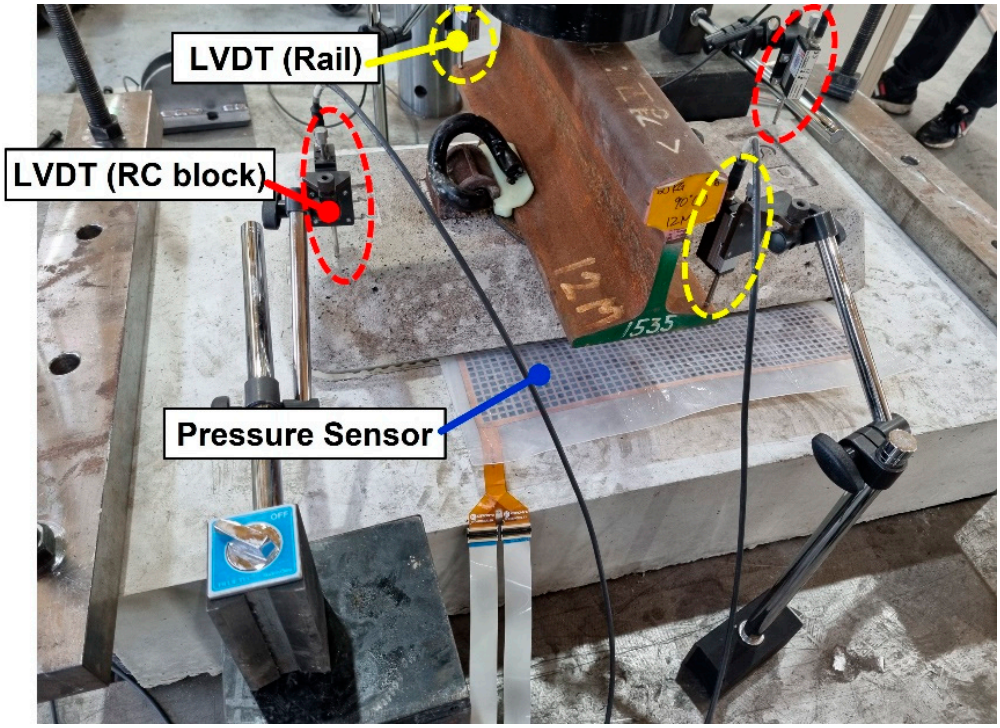


Figure 9. Measurement sensors installed.

3.2. Laboratory Test Condition

In this study, static and dynamic loading tests were conducted. The static loading test was conducted in accordance with Korean Railway Standards [13]. For the static loading test, the magnitude of the load ranged from 1 to 64 kN, and loading was performed three times. In the case of the dynamic loading test, the average load was set to 80 kN under four conditions. The load conditions of the static loading test are shown in Figure 10a, and the load conditions of the dynamic loading test are shown in Figure 10b. Table 2 shows the conditions for the static and dynamic loading tests.

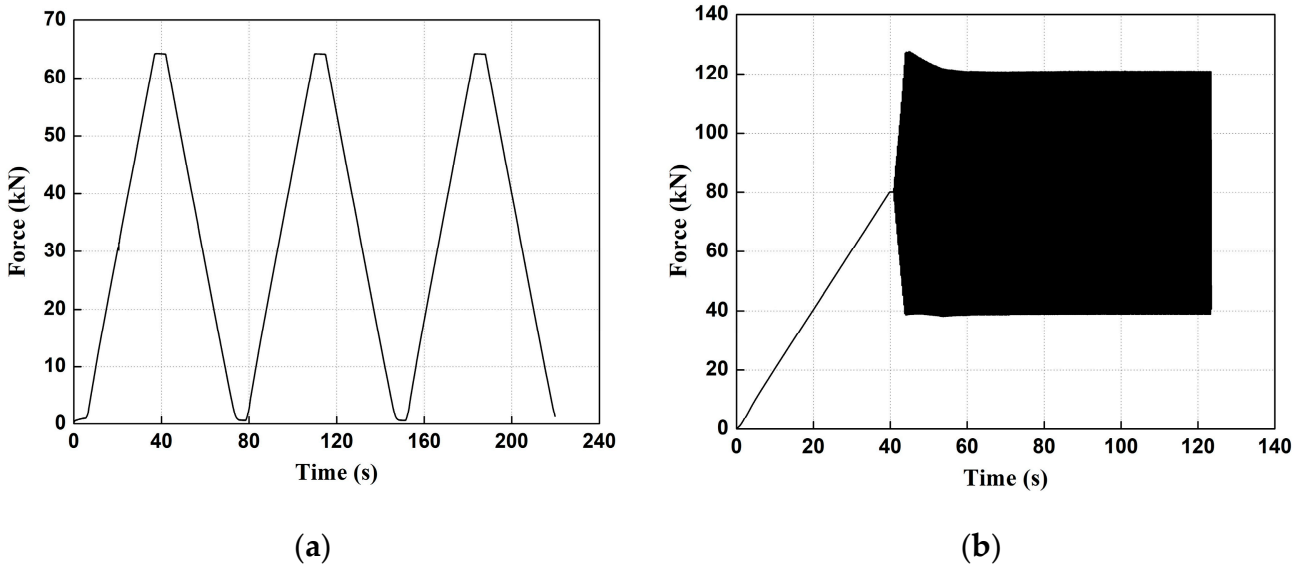


Figure 10. Laboratory test load condition: (**a**) static loading test; (**b**) dynamic loading test.

Table 2. Laboratory test load condition.

Laboratory Test Condition		Mean Load (kN)	Load Amplitude (kN)	Min. Load (kN)	Max. Load (kN)	Frequency (Hz)	Number of Cycles
Static loading test		-	-	1	64	-	3
Dynamic loading test	Load case 1 (±10%)	80	±8	72	88	4	250
	Load case 2 (±25%)	80	±20	60	100	4	250
	Load case 3 (±40%)	80	±32	48	112	4	250
	Load case 4 ($\pm TIF_{Design}$)	80	±41.04	38.96	121.04	4	250

In this study, conditions for the dynamic loading test were set as shown in Table 2. Laboratory tests were conducted by setting 10%, 25%, 40%, and 51.3% of the average load as load amplitudes for the dynamic loading test, as shown in Table 2. In load case 4, the load amplitude was set to 51.3%, considering a maximum track impact factor of 1.513 (V = 100 km/h) for urban railway design in South Korea as the maximum load condition.

3.3. Laboratory Test Results

3.3.1. Static Loading Test

In this study, laboratory tests were conducted to analyze the change in pressure at the bottom of the sleeper for both new resilience pads and pads that had been used for more than ten years among the STEDEF components. The laboratory tests were conducted according to the KR standard in this study. The main measurements for this test were the vertical displacements of the rail and sleeper as well as the pressure at the bottom of the sleeper. Before the pressure measurement, the difference in spring stiffness between new and used resilience pads was analyzed. The rail support spring stiffness was calculated using the laboratory test load and the measured vertical displacement of the rail. The measured vertical displacement of the sleeper was used for a comparative analysis with the numerical analysis results. The pressure at the bottom of the sleeper was also used for a comparative analysis with the measurement and analysis results. Figure 11 shows the load–displacement graphs obtained through laboratory tests on new and used resilience pads.

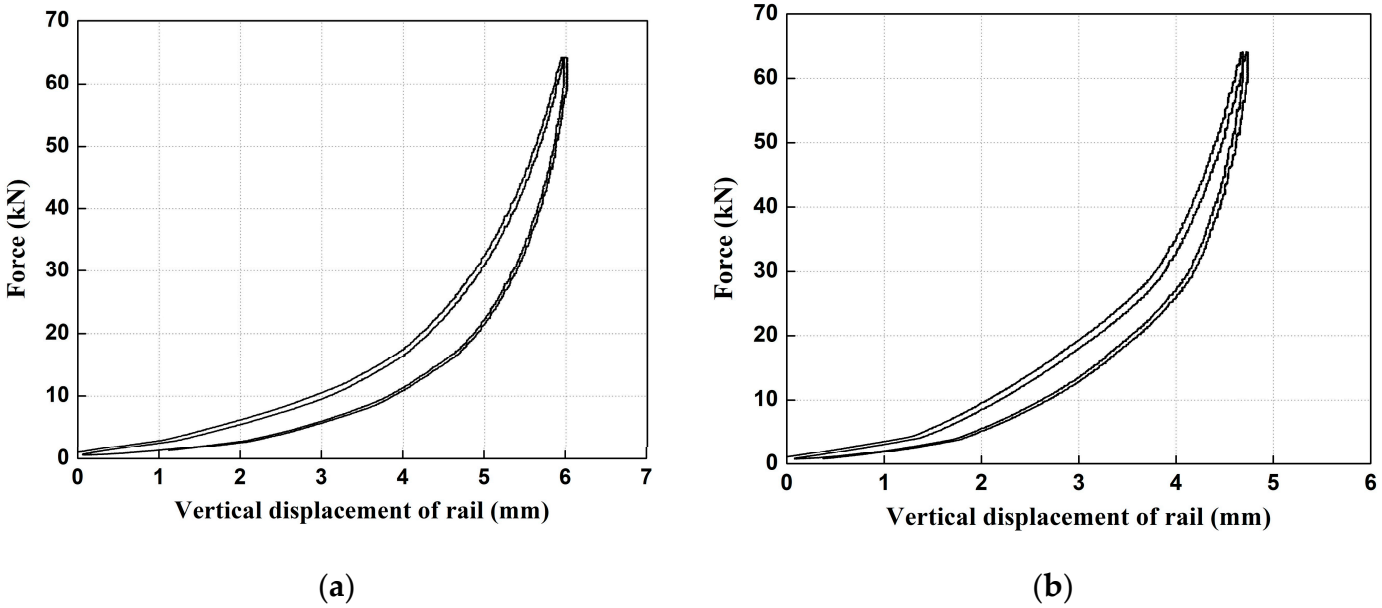


Figure 11. Static loading test results (load–vertical displacement): (**a**) resilience pad (new); (**b**) resilience pad (used).

In this study, the load–displacement relationship was obtained via tests on the STEDEF assembly, as shown in Figure 11. The rail support and resilience pad spring stiffness values were calculated based on the measured load and vertical displacement of the rail. The equation used to calculate the rail support spring stiffness using the laboratory test data was as follows [13]:

$$k_{SA} = \frac{F_{SA2} - F_{SA1}}{d_{SA}}, \text{ kN/mm} \quad (F_{SA2} = 0.8F_{SAmax}), \tag{6}$$

where F_{SA1} is the minimum load applied to the assembly during the static stiffness test, F_{SAmax} is the maximum load applied to the assembly during the static stiffness test, k_{SA} is the rail support spring stiffness, and d_{SA} is the average vertical displacement of the assembly. The theoretical rail support spring stiffness calculation formula is given as follows [13].

$$k_{SA} = \frac{1}{\frac{1}{k_1} + \frac{1}{k_2} + \frac{1}{k_3}}, \tag{7}$$

where k_1 is the spring stiffness of the rail pad, k_2 is the spring stiffness of the resilience pad, and k_3 is the spring stiffness of the rubber boots [13]. In this study, the rail support spring stiffness k_{SA} was calculated using laboratory test data via Equation (1), and the spring stiffness of the resilience pad was calculated using Equation (2) [1,2,6]. In this case, 400 and 2000 kN/m were applied as the spring stiffness values of the rail pad and rubber boots, respectively, through the application of the design specifications [1,2,6]. Table 3 is the static loading test results.

Table 3. Static loading test results (assembly).

Load Condition	New		Used	
	Force (kN)	Average Rail Displ. (mm)	Force (kN)	Average Rail Displ. (mm)
F_{sa2}	51.2	4.72	51.2	3.64
F_{sa1}	1.0		1.0	

The rail support spring stiffness was analyzed to be approximately 10.64 and 13.79 kN/mm under the application of new and used resilience pads, respectively. The static vertical stiffness was also analyzed to be approximately 10.99 and 14.39 kN/mm, respectively. The spring stiffness of the used resilience pad was approximately 31% higher than that of the new resilience pad. In the case of the new resilience pad, the average rail displacement was analyzed to be approximately 4.72 mm.

Figure 12 shows the measurement results of the pressure at the bottom of the concrete sleeper that were obtained using the pressure sensor under the new-resilience-pad condition.

When the pressure was measured using the pressure sensor, the maximum pressure was observed to be approximately 2.20 MPa for the new resilience pad, as shown in Figure 12. The maximum pressure for the used resilience pad was approximately 2.44 MPa. An analysis of the measurement results for the new and used resilience pads showed that the region with a pressure of 1.07–1.43 MPa was similar for both the new and used resilience pads. The region with a pressure of 2.14 MPa or higher was larger in the used resilience pad compared to that of the new resilience pad.

In this study, laboratory tests on new and used resilience pads were conducted using the pressure sensor. Linear regression analysis was also conducted using the measurement results. As observed in Figure 13, the linear regression analysis results for the static loading test showed that the slope of the pressure versus load graph for the used resilience pad was approximately 1.13 times higher than that of the new resilience pad. This indicates that the pressure at the bottom of the sleeper increased owing to an increase in the spring stiffness of the resilience pad.

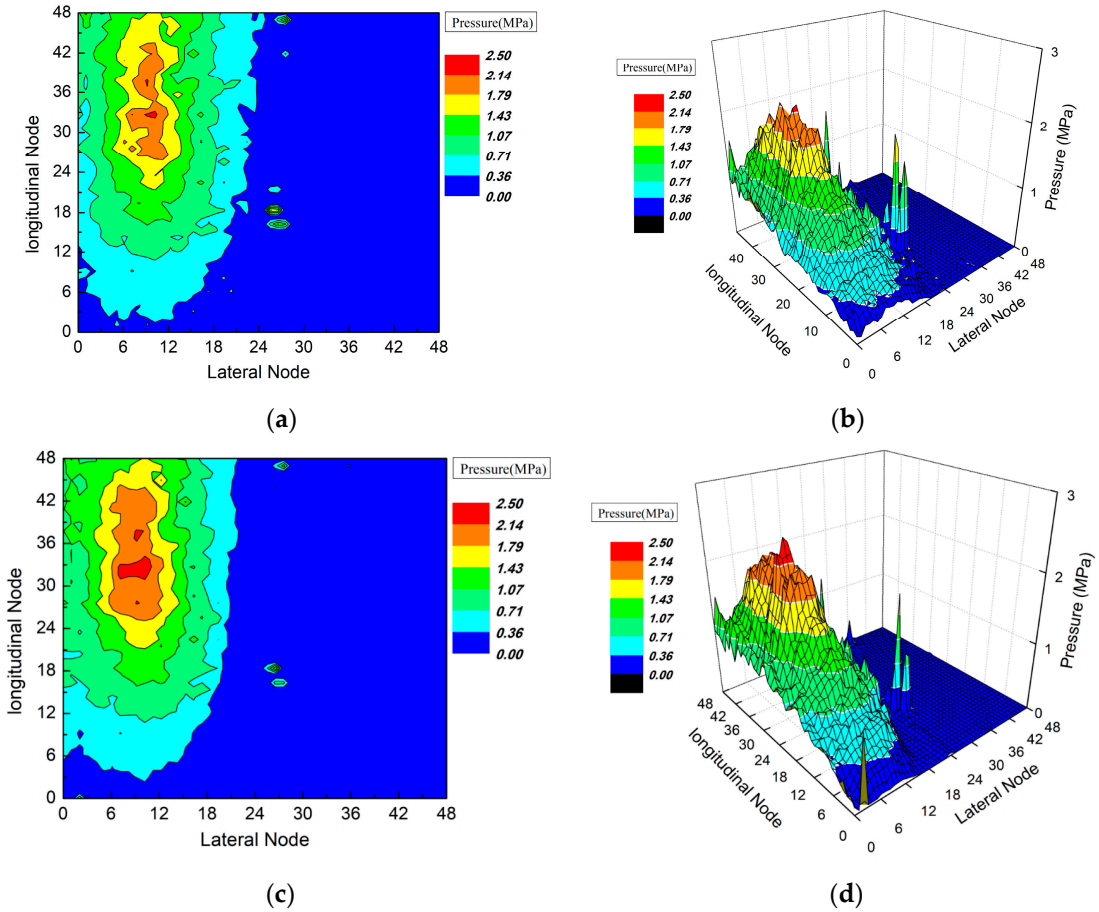


Figure 12. Static loading test results (under the application of the maximum static load): (**a**) pressure contour (2D, new resilience pad); (**b**) pressure contour (3D, new resilience pad); (**c**) pressure contour (2D, used resilience pad); (**d**) pressure contour (3D, used resilience pad).

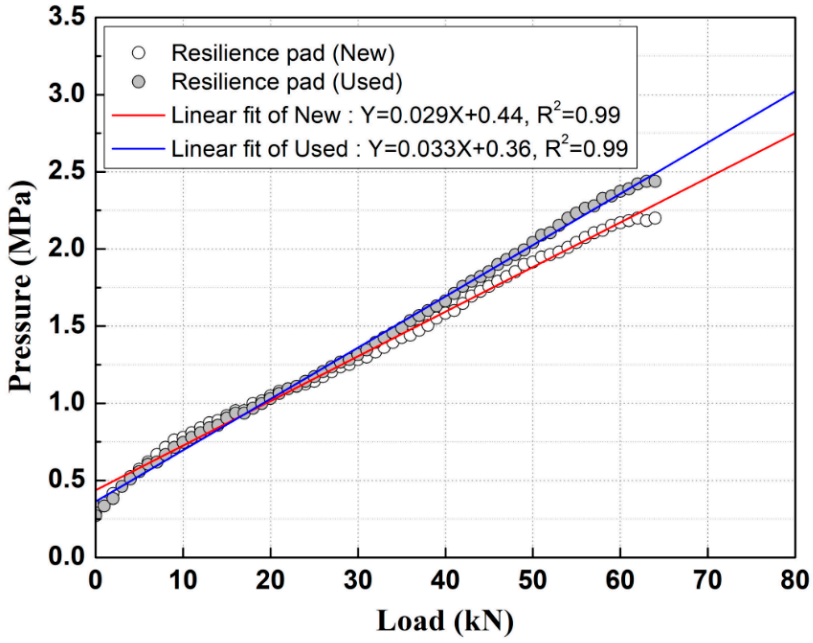


Figure 13. Static loading test measurement results (new and used resilience pads).

3.3.2. Dynamic Loading Test

In this study, the dynamic loading test was conducted to analyze the influence of new and old resilience pads on the pressure measurements. Through this test, the pressure values at the bottom of the sleeper for the new and used resilience pads were compared, and the measurement performance of the pressure sensor was analyzed.

The pressure at the bottom of the sleeper was measured using the pressure sensor. Figure 14 shows the measurement results for the new resilience pad.

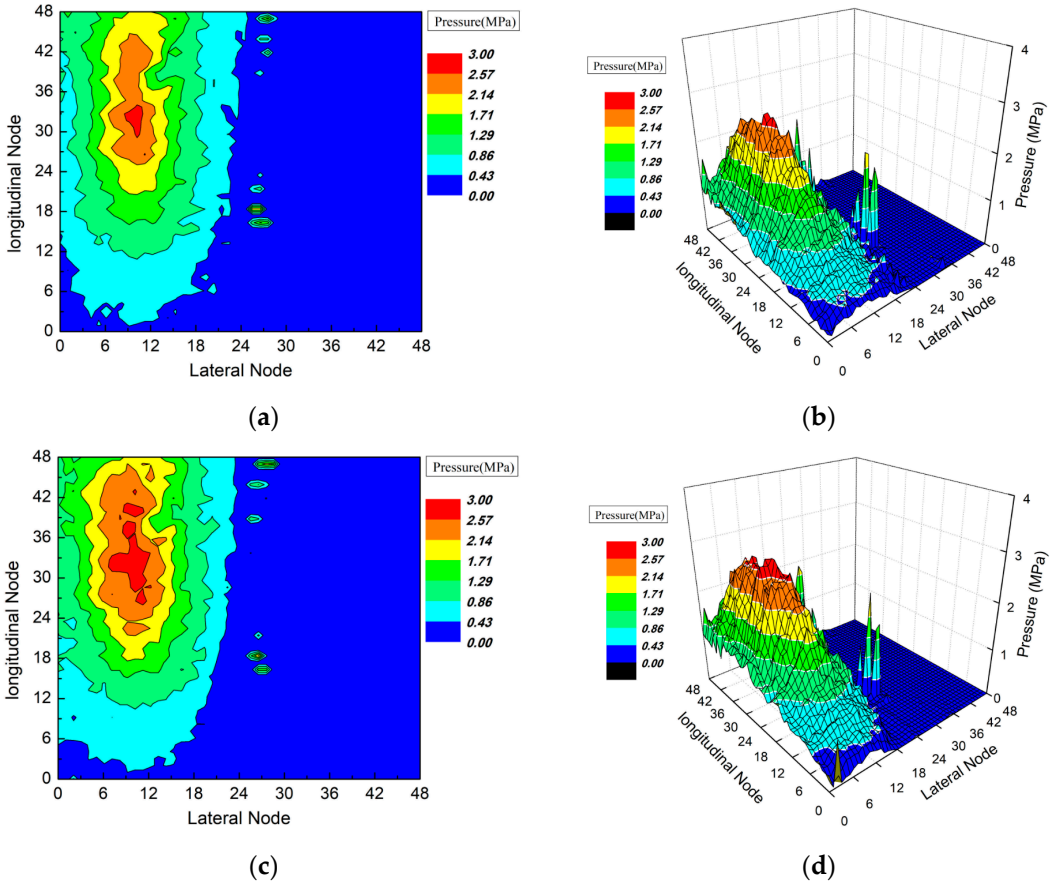


Figure 14. Dynamic loading test results (load case 4): (**a**) pressure contour (2D, new resilience pad); (**b**) pressure contour (3D, new resilience pad); (**c**) pressure contour (2D, used resilience pad); (**d**) pressure contour (3D, used resilience pad).

Figure 14 shows the pressure measurement results under the maximum load during the dynamic loading test for each resilience pad (load case 4). As shown in Figure 14a,c, the 2D measurement results showed a difference in the region with a pressure of 2.57 MPa or higher, which depended on the spring stiffness. Figure 14b,d are the three-dimensional (3D) graphs of pressure generated at each node of the pressure sensor. For the new resilience pad, the pressure-measurement results in the dynamic test results (load case 4) were approximately 27.3% higher than that of the static test results in Figure 12. In the case of the used resilience pad, the pressure-measurement results in the dynamic test results (load case 4) were approximately 20.9% higher than that of the static test results. This indicates that an increase in resilience pad spring stiffness directly caused an increase in the pressure at the bottom of the sleeper.

Figure 15 shows the pressure-measurement results during the dynamic loading test.

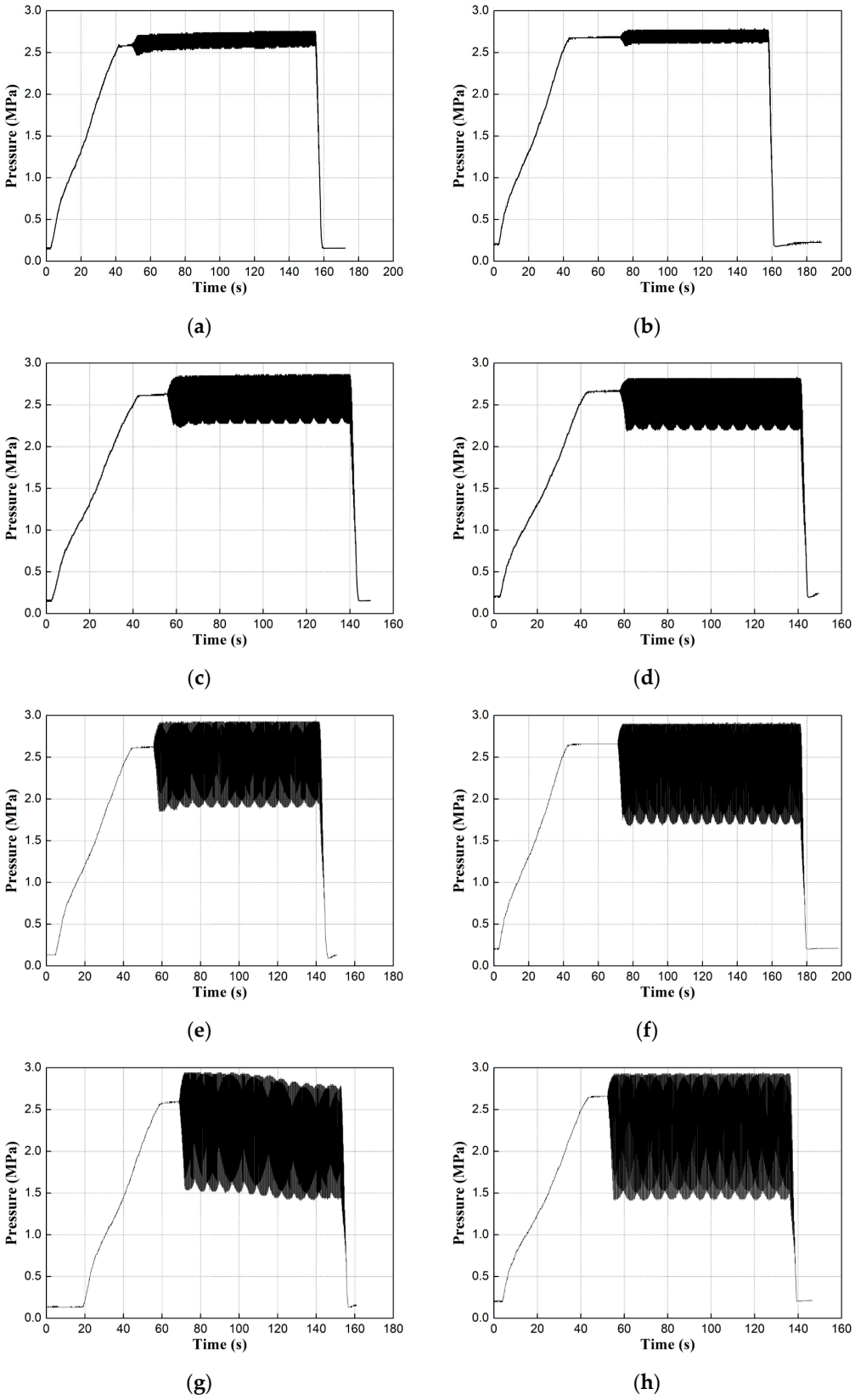


Figure 15. Dynamic loading test measurement results: (**a**) load case 1, new resilience pad; (**b**) load case 1, used resilience pad; (**c**) load case 2, new resilience pad; (**d**) load case 2, used resilience pad; (**e**) load case 3, new resilience pad; (**f**) load case 3, used resilience pad; (**g**) load case 4, new resilience pad; (**h**) load case 4, used resilience pad.

As shown in Table 4, the minimum load decreased and the maximum load increased as the load amplitude increased. Therefore, in the pressure-measurement results, the minimum pressure of load case 1 was approximately 82% higher than that of load case 4 for the new resilience pad, as shown in Table 4. In addition, the maximum pressure of load case 1 was approximately 2.1% lower than that of load case 4. In the case of the used resilience pad, the minimum pressure of load case 1 was approximately 85% higher than that of load case 4, whereas the maximum pressure of load case 1 was approximately 6.1% lower than that of load case 4.

Table 4. Dynamic loading test analysis results.

Load Case	Resilience Pad (New)		Resilience Pad (Used)	
	Min (MPa)	Max (MPa)	Min (MPa)	Max (MPa)
case 1 (±10%)	2.55	2.74	2.61	2.77
case 2 (±25%)	2.20	2.81	2.20	2.82
case 3 (±40%)	1.82	2.90	1.70	2.91
case 4 ($\pm TIF_{Design}$)	1.40	2.80	1.41	2.95

The maximum and minimum pressure analysis results in load cases 1–4 for each resilience pad are shown in Figure 16.

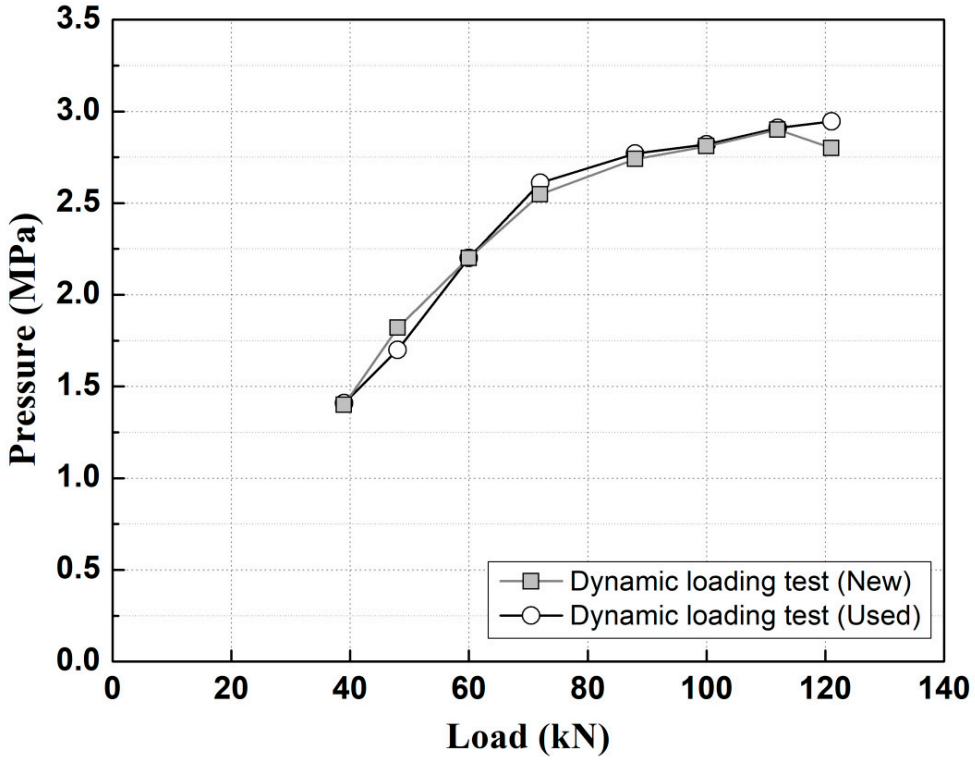


Figure 16. Dynamic loading test results (measured pressure).

The dynamic test pressures of the new and used resilience pads were compared, as shown in Figure 16. The dynamic loading test results showed that the pressure of the used resilience pad was higher than that of the new resilience pad, except for a load of 48 kN. It was also observed that the new and used resilience pads had similar tendencies up to 112 kN. However, when a maximum of 121.04 kN was applied, the pressure difference between the new and used resilience pads was analyzed to be approximately 0.15 MPa. Under a maximum load of 121.04 kN, the pressure of the used resilience pad was approximately 5.4% higher than that of the new resilience pad.

New products have lower spring stiffness compared with the used products. This is attributed to the difference in the elastic restoring force when the maximum load of 121.04 kN is applied at the speed of 4 Hz.

Accelerated aging and fatigue tests were not performed for the resilience pads used in the experiment. This phenomenon can be attributed to the nonlinear behavioral characteristics of the rubber material.

Additionally, we cannot rule out the occurrence of errors in measuring sensors. However, the static test results match the logic proposed in this study. Thus, we shall be able to identify the cause if additional research is conducted for the condition in which dynamic loads are applied.

4. Finite Element Analysis

4.1. Overview

In this study, numerical analysis was conducted through the analytical modeling of 3D solid elements, from the rail to the concrete bed. In general, pressure is the applied load divided by the cross-sectional area. This study analyzed the magnitude and geometry of the pressure (stress) generated at the bottom of the resilience pad under the application of a load. ANSYS Workbench Ver. 2023 R1, a general-purpose structural analysis software program, was used for the numerical analysis [14].

4.2. Modeling

This study analyzed the magnitude and geometry of the pressure generated at the bottom of the concrete sleeper, which was one of the STEDEF components. To ensure a behavior analysis that is similar to reality, the rail, rail pad, concrete sleeper, rubber boots, and concrete bed were set as 3D solid elements. Solid-element analysis was required to analyze the geometry of the pressure generated under the resilience pad. Figure 17 shows the schematic of the STEDEF. In addition, the specifications of the STEDEF components used in the numerical analysis are shown in Table 5.

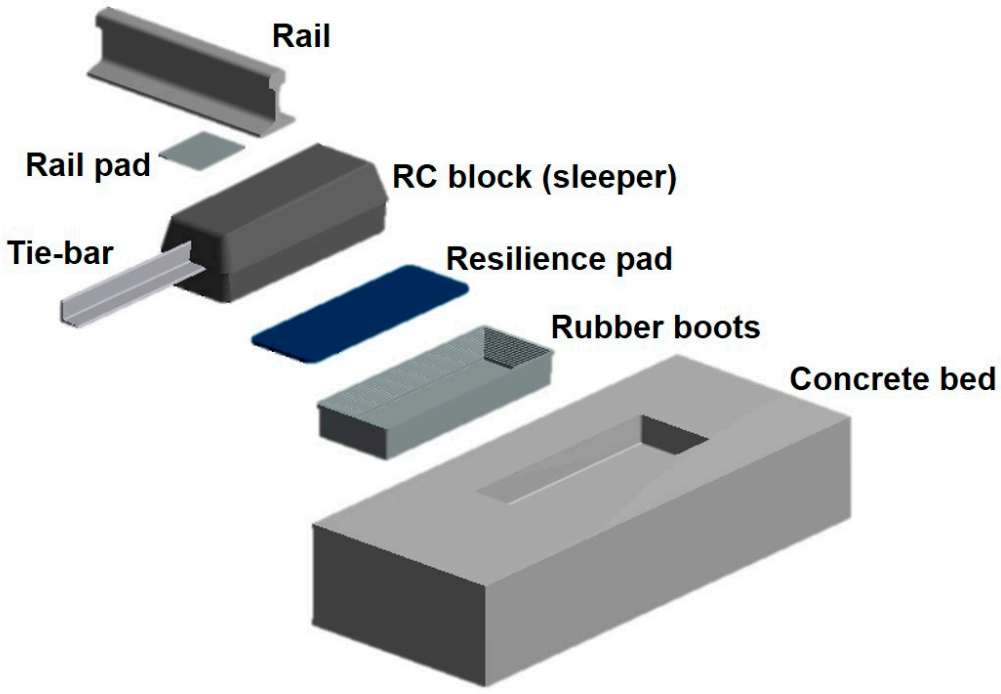


Figure 17. Schematic of the booted sleeper track system (STEDEF) [6].

Table 5. Material properties of the booted sleeper track (STEDEF) system components [6].

Component	Properties		Resilience Pad (Used)	
	Size	**Density (kN/m^3)**	**Elastic Modulus (MPa)**	**Poisson's Ratio (υ)**
Rail	I = 3090 cm^4 A = 77.5 cm^2	77.01	210,000	0.3
Rail pad	Size = 190 × 193 mm Thickness = 5 mm	9.32	71.4	0.2
RC block	Size = 257 × 684 mm Height = 205 mm	22.56	26,086	0.18
Tie-bar	Size = 65 × 65 mm Length = 2000 mm	77.01	200,000	0.3
Resilience pad	Size = 230 × 660 mm Thickness = 12 mm	6.87	-	0.49
Rubber boots	Height = 100 mm Thickness = 5 mm	7.85	2000	0.2
Concrete bed	Width = 3000 mm Height = 300 mm	22.56	26,086	0.18

In numerical analysis modeling, all the components, from the rail to the concrete bed, were set as 3D solid elements. To verify the validity of the model, the model was set under the same conditions as those of the laboratory tests. Figure 18 shows the numerical analysis model, load conditions, and boundary conditions. For the boundary conditions between track components, rail and rail pad, rail pad and RC block, RC block and tie-bar, and rubber boots and concrete bed have a bonded condition, RC block and rubber boots, and RC block—a frictional condition was applied for resilience pads, but no condition was applied for resilience pads and rubber boots.

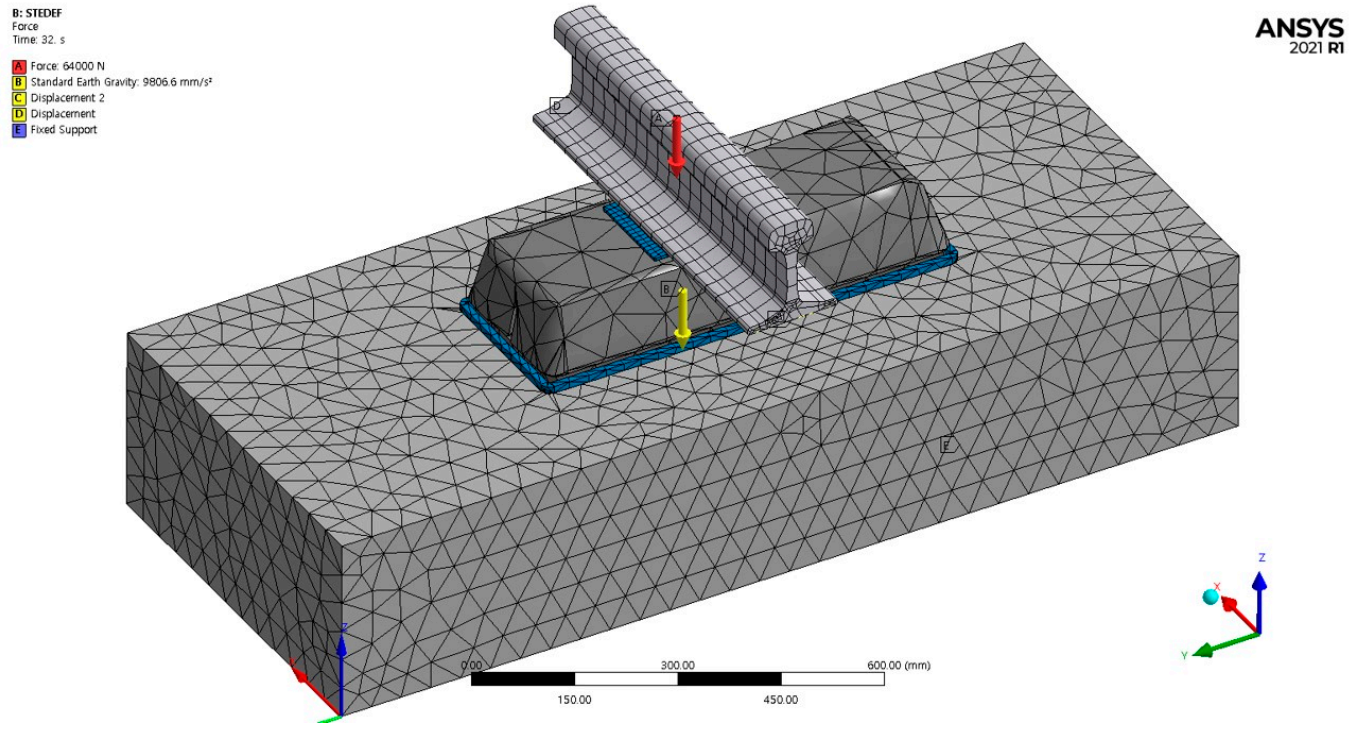


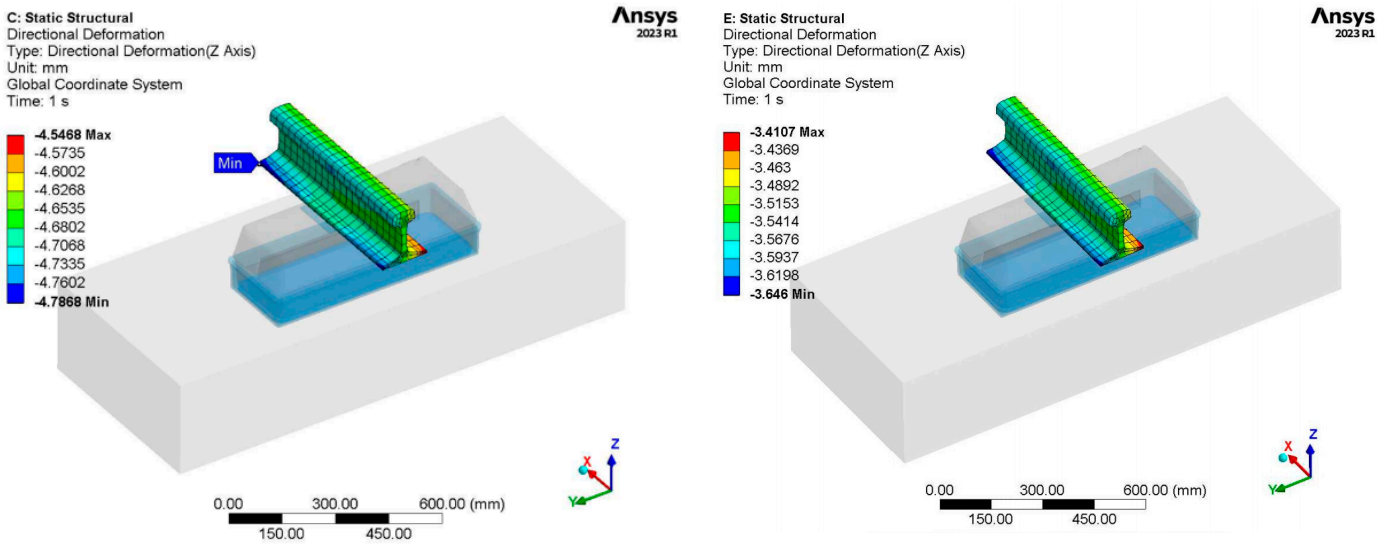
Figure 18. FE model of the booted sleeper track system (boundary and load conditions).

The numerical analysis model contained 55,846 nodes and 28,574 elements. In the boundary conditions, the lower surface of the concrete bed was set as a fixed support. For both ends of the rail, the X and Y axes were fixed, and the Z axis was set to be free. The load position was set to the center of the rail head. The load conditions were set between 0 and 64 kN, in the same manner as in the static loading test.

4.3. Analysis Result

In most of the previous studies, resilience pads were used for analysis as spring elements. However, in this study, the elastic modulus was required for analysis because the resilience pad was a solid element. The analysis and laboratory test results were compared to calculate the appropriate elastic modulus of the resilience pad.

The analysis and laboratory test results were compared and analyzed to verify the validity of the numerical analysis results. The vertical displacement of the rail was compared between the laboratory test and analysis results. Figure 19 shows the measurement and analysis results.

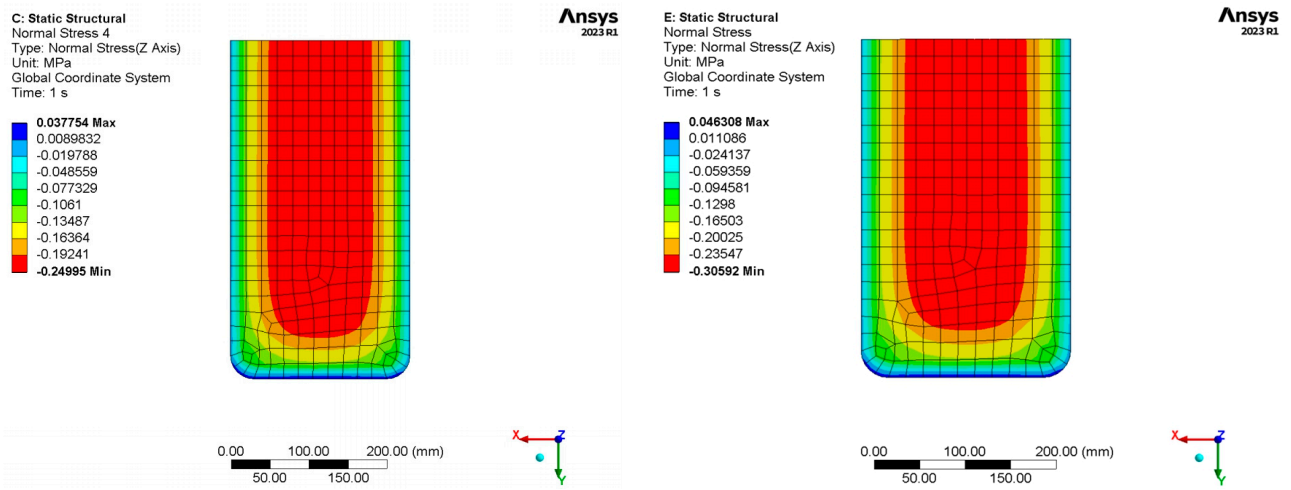


(**a**) (**b**)

Figure 19. Analysis results for the vertical displacement of rail: (**a**) new resilience pad; (**b**) used resilience pad.

As shown in Figure 19, the vertical displacement of the rail was compared between the numerical analysis and laboratory test results. For the new resilience pad, the vertical displacement of the rail was observed to be approximately 4.72 mm in the laboratory tests and 4.78 mm in the numerical analysis. The error between the numerical analysis and laboratory test results was approximately 1.3%; therefore, the analysis model was judged to be appropriate. In this case, 0.08 MPa was used as the elastic modulus of the new resilience pad. In the case of the used resilience pad, the vertical displacement of the rail was observed to be approximately 3.64 mm for the laboratory tests and 3.65 mm for the numerical analysis. The analysis model was judged to be appropriate because the error between the analysis and laboratory test results was approximately 0.3%. In this case, 0.125 MPa was used as the elastic modulus of the used resilience pad.

The numerical analysis results for each resilience pad are shown in Figure 20.



(**a**) (**b**)

Figure 20. Numerical analysis results (normal stress, z axis): (**a**) new resilience pad; (**b**) used resilience pad.

In this study, the compressive stress for each resilience pad was analyzed via numerical analysis, as shown in Figure 21. The maximum compressive stress of the new resilience pad was analyzed to be approximately 0.25 MPa, whereas that of the used resilience pad was approximately 0.306 MPa. The compressive stress of the used resilience pad was approximately 22.4% higher than that of the new resilience pad.

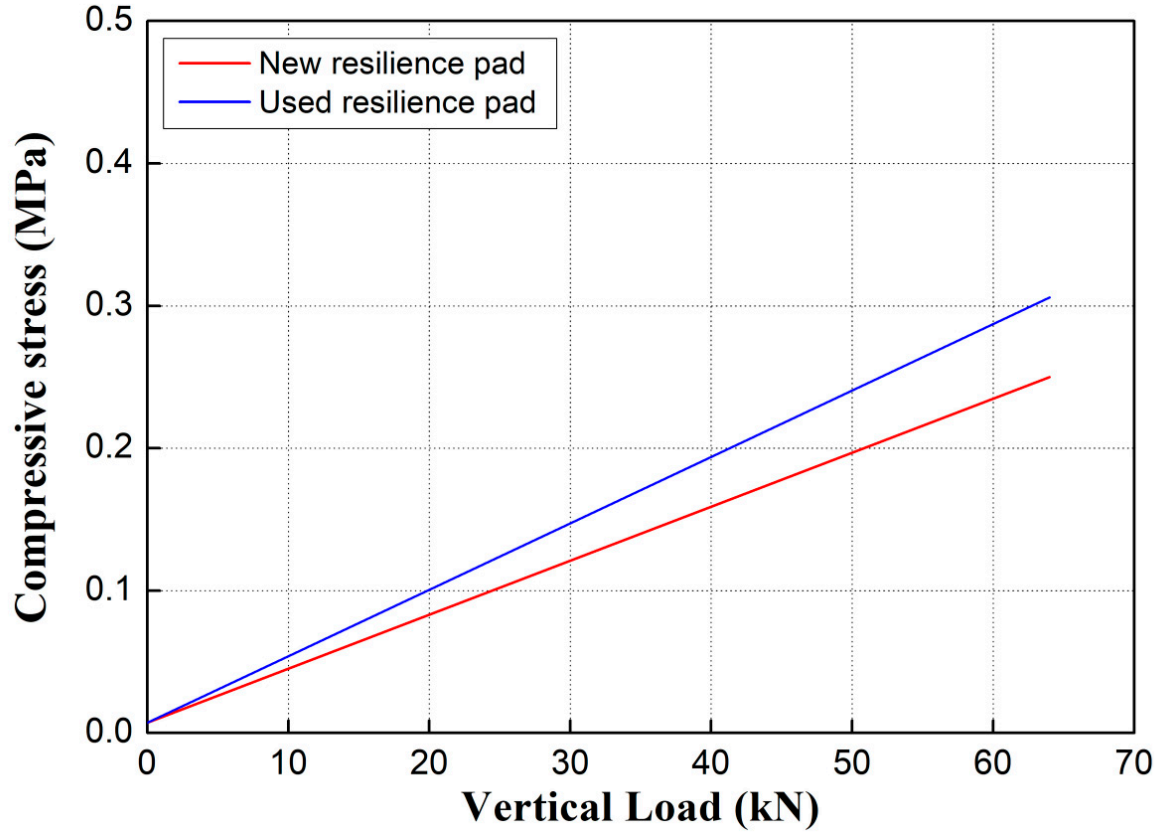
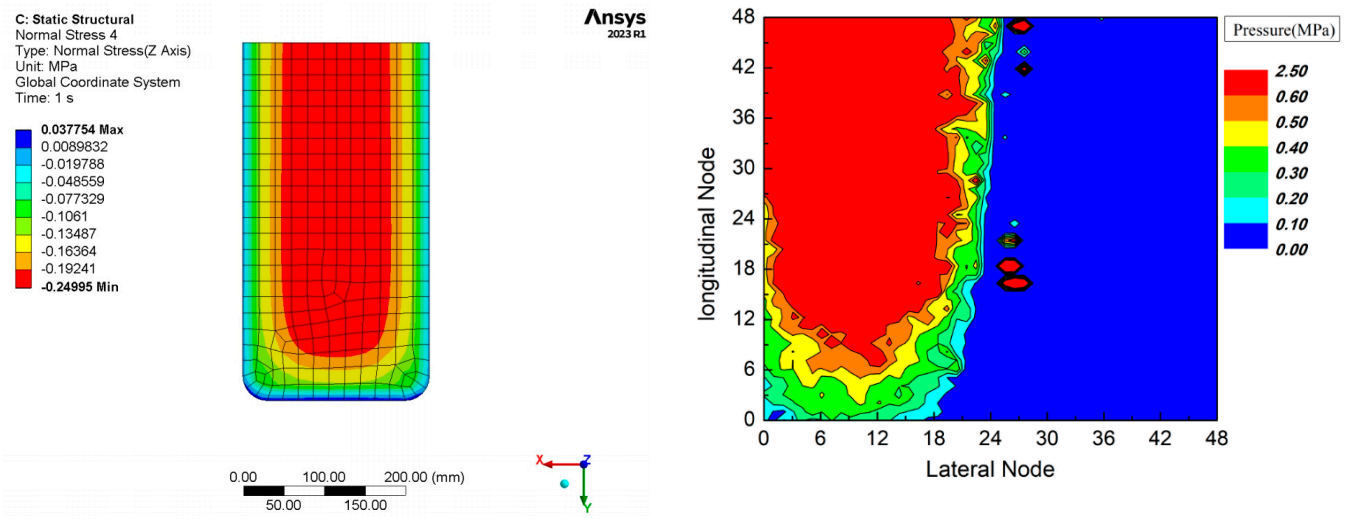


Figure 21. Compressive stress analysis results for each resilience pad.

Figure 22 compares the analysis and laboratory test results for the new resilience pad.



(**a**) (**b**)

Figure 22. Comparison between the numerical analysis and laboratory test results for the new resilience pad: (**a**) compressive stress analysis results (normal stress, z axis); (**b**) pressure sensor measurement results (laboratory test).

The numerical analysis and laboratory test results for the new resilience pad were compared, as shown in Figure 22. In the case of the numerical analysis results, the same area as that measured when installing the pressure sensor was analyzed. The pressure sensor measurement and numerical analysis results exhibited similar contours. The maximum local compressive stress was 0.38 MPa in the numerical analysis. In the static laboratory test results for the new resilience pad, the maximum pressure was 2.21 MPa. Thus, a considerable difference in stress (pressure) was observed between the numerical analysis and laboratory test results. For the pressure sensor, the pressure was measured from the 5 × 5 mm node. However, in the case of the numerical analysis, the stress was measured from a 20 × 20 mm area with a thickness of 12 mm. Because the pressure was determined by the area, the load acting on the actual node was calculated instead of the pressure. When an area of 25 (5 × 5 mm) mm^2 was considered for the maximum pressure measured from the pressure sensor, the load acting on the node was 55.25 N. When an area of 240 (20 × 12 mm) mm^2 was considered for the stress analyzed through the numerical analysis, the load acting on the node was analyzed to be 59.98 N.

Figure 23 shows the results of converting the pressures measured through the numerical analysis and laboratory tests into the load acting on the node.

As shown in Figure 23, the correlation between the resilience pad compressive stress and the load on each node was analyzed. Under initial loads, the load on each node analyzed through the laboratory tests was higher than that on each node obtained through the numerical analysis. However, under the maximum load on the rail, the load on each node obtained through the numerical analysis was approximately 4.73 N higher than that of the laboratory tests. Compared to the laboratory tests, the load on each node obtained through the numerical analysis was different by approximately 7.9%.

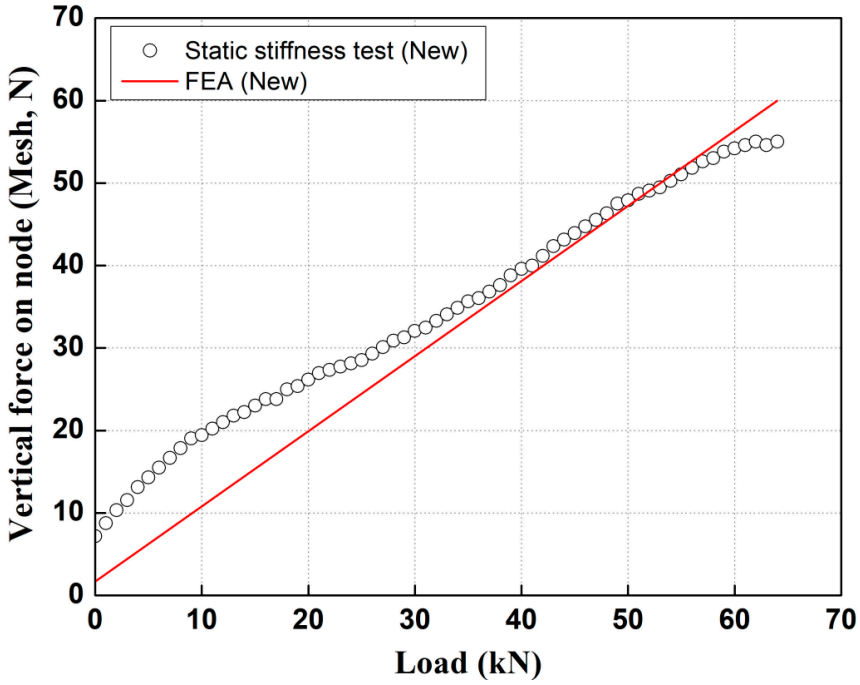


Figure 23. Analysis results showing the correlation between the resilience pad compressive stress and the load on each node.

5. Results and Discussion

5.1. Overview

In this study, laboratory tests on the STEDEF assembly were conducted to verify the performance of the pressure sensor. The pressure values measured through laboratory tests were compared with the numerical analysis results. In addition, we proposed a process for evaluating the spring stiffness of resilience pads in the STEDEF using a pressure sensor.

5.2. Comparison between Laboratory Test and Numerical Analysis Results

The results of laboratory tests that used the pressure sensor were compared with the numerical analysis results, as shown in Figure 24.

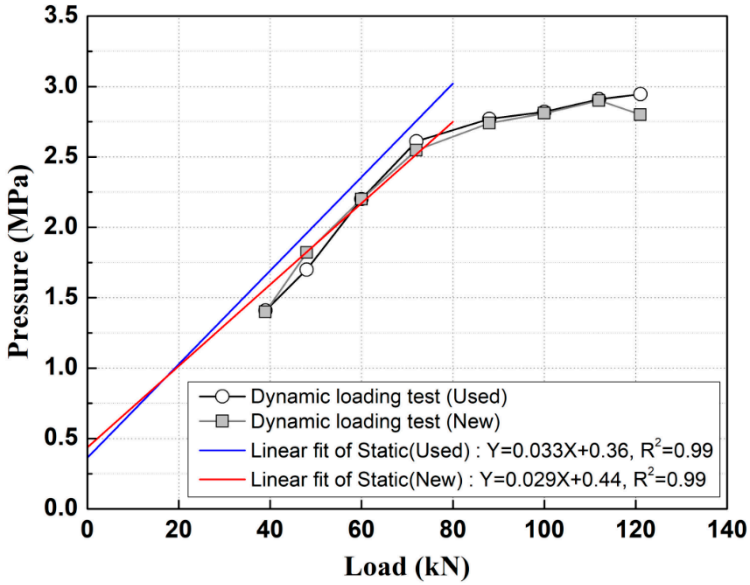


Figure 24. Laboratory test analysis results (static and dynamic).

As shown in Figure 24, the dynamic test results showed that the pressure at the bottom of the sleeper linearly increased as the load increased from 0 to 70 kN. However, as the load exceeded approximately 70 kN, the pressure gradient according to the load decreased. Therefore, the pressure levels of the static and dynamic tests were similar for up to approximately 70 kN. However, from 70 kN onwards, the linear regression gradient was different from the gradient of the dynamic test results.

The linear regression line for the static test results was compared with that of the dynamic test results, as shown in Figure 24. The comparison showed that the pressure did not linearly increase proportionally to the increase in the test load. The results under the minimum loads of load cases 1–4, which are dynamic test conditions, were compared with the static test results. In load case 1, the static laboratory test pressure was approximately 0.8% higher than that of the dynamic laboratory test for the new resilience pad. However, in the case of the used resilience pad, the static laboratory test pressure was approximately 4.6% lower than that of the dynamic laboratory test. In load case 4, the static laboratory test pressure was approximately 10.2% lower than that of the dynamic laboratory test for the new resilience pad. In the case of the used resilience pad, the static laboratory test pressure was also approximately 14.9% lower than that of the dynamic laboratory test.

5.3. Method to Improve the Resilience Pad Spring Stiffness Evaluation Technique

This study proposed a method to improve the evaluation technique for the spring stiffness of resilience pads in the STEDEF. In general, track performance was evaluated through the track support stiffness and track impact factor calculation results. Track performance was evaluated based on the spring stiffness results of elastic materials (elastic pads), which are key elements among the track components.

An anomaly-detection system process for SOC facilities using a pressure sensor is shown in Figure 25.

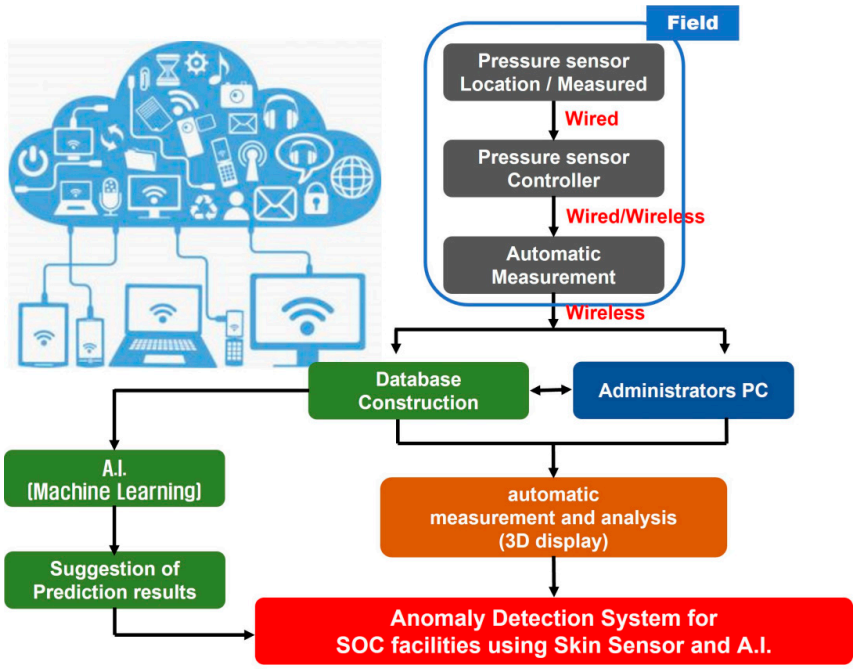


Figure 25. Anomaly-detection system process for SOC facilities using a pressure sensor.

A pressure sensor and automatic measurement system were installed in the field, and data measurements were obtained. The measured data were stored in a database and transmitted to the administrator PC. For the analysis of the measurement results, machine learning analysis was conducted based on the data stored in the database to evaluate the behavior of SOC facilities. In addition, the measured data were examined using 3D display

software. Moreover, an anomaly-detection system for facilities can be constructed using a pressure sensor through the process shown in Figure 25.

6. Conclusions

This study proposed a technique to evaluate the spring stiffness of resilience pads in the booted sleeper track system (STEDEF) using a pressure sensor. Previous studies used a strain gauge to measure the wheel load, and LVDT to measure the vertical displacement of rail and sleepers. Then, spring stiffness at the rail support point was estimated using the measurements. However, this study used a pressure sensor to measure the pressure acting on the resilience pads. Pressure is a factor determining the reaction force at the support point and indicates the changes in spring stiffness at the rail support point. In other words, the purpose of this study was to estimate the spring stiffness of resilience pads by measuring the pressure. Laboratory tests showed that the pressure at the bottom of the sleeper increased owing to the aging (spring stiffness increase) of resilience pads in the STEDEF. Therefore, we experimentally verified that the change in the spring stiffness of resilience pads in the STEDEF can be detected using a pressure sensor. Numerical analysis showed that an increase in the spring stiffness of the resilience pads had a direct impact on the increase in pressure at the bottom of the sleeper and the stress of the resilience pads. The analysis model was proven to reflect the experimental conditions well because it exhibited very similar results to those of the experiment. It is possible to determine an increase or decrease in the spring stiffness of resilience pads based on the pressure generated in the new resilience pad. This can be utilized when evaluating the deterioration and uplift of sleepers. The STEDEF is a track type in which changes in the sleeper support conditions and the spring stiffness of resilience pads cannot be easily identified according to the uplift and settlement of underground structures. Therefore, the use of the proposed technique will make it possible to evaluate the sleeper support conditions of the STEDEF and the spring stiffness of resilience pads together. In addition, this real-time monitoring technique will be highly useful for tracking maintenance because the deterioration process of resilience pads can be monitored for railways in operation based on the pressure at the bottom of the sleeper. Given that this study derived the results at the laboratory level, additional research is needed to propose the replacement period for resilience pads. Thus, it is required to conduct additional studies to (1) validate the suitability of a pressure sensor based on a field test and (2) analyze the correlation between spring stiffness and pressure considering the nonlinear behavior of resilience pads based on fatigue tests. Therefore, conducting additional studies will help propose more accurate results on the replacement period of resilience pads.

Author Contributions: Conceptualization, J.-Y.C., D.-H.A. and J.-S.C.; methodology, J.-S.C. and J.-M.H.; software, D.-H.A. and J.-M.H.; formal analysis, J.-Y.C. and J.-S.C.; investigation, J.-Y.C. and J.-M.H.; data curation, J.-Y.C., D.-H.A. and J.-M.H.; writing—original draft preparation, J.-Y.C. and D.-H.A.; writing—review and editing, D.-H.A. All authors have read and agreed to the published version of the manuscript.

Funding: This work was supported by the Institute of Information & Communications Technology Planning & Evaluation (IITP) grant funded by the Korean government (MSIT) (No.2022-0-00829, Development of Real-time Anomaly Detection System for SOC facilities using Skin Sensors and A.I.).

Institutional Review Board Statement: Not applicable.

Informed Consent Statement: Not applicable.

Data Availability Statement: Data sharing is not applicable to this article.

Conflicts of Interest: The authors declare no conflict of interest.

References

1. Choi, J.Y.; Kim, S.H.; Kim, M.H.; Chung, J.S. Development of track support stiffness measurement and evaluation system for slab tracks. *Appl. Sci.* **2020**, *10*, 4344. [CrossRef]
2. Choi, J.Y. Qualitative Analysis for Dynamic Behavior of Railway Ballasted Track. Ph.D. Thesis, Technical University of Berlin, Berlin, Germany, 2014.
3. Li, J.; Zhang, J.; Yang, X.; Zhang, A.; Yu, M. Monte Carlo simulations of deformation behaviour of unbound granular materials based on a real aggregate library. *Int. J. Pavement Eng.* **2023**, *24*, 2165650. [CrossRef]
4. Fu, H.; Yang, Y.; Kaewunruen, S. Multi-Hazard Effects of Crosswinds on Cascading Failures of Conventional and Interspersed Railway Tracks Exposed to Ballast Washaway and Moving Train Loads. *Sensors* **2023**, *23*, 1786. [CrossRef] [PubMed]
5. Nacaratnarajah, S.K.; Mayuranga, H.G.S.; Venuja, S. Influence of Type of Sleeper–Ballast Interface on the Shear Behaviour of Railway Ballast: An Experimental and Numerical Study. *Sustainability* **2022**, *14*, 16384. [CrossRef]
6. Choi, J.Y.; Ahn, D.H.; Kim, S.H. Behavior characteristics of a booted sleeper track system according to substructure deformation. *Appl. Sci.* **2021**, *11*, 4507. [CrossRef]
7. Hannan, A.; Shafiq, M.Z.; Hussain, F.; Pires, I.M. A portable smart fitness suite for real-time exercise monitoring and posture correction. *Sensors* **2021**, *21*, 6692. [CrossRef] [PubMed]
8. Menzel, T.; Potthast, W. Validation of a novel boxing monitoring system to detect and analyse the centre of pressure movement on the boxer's fist. *Sensors* **2021**, *21*, 8394. [CrossRef] [PubMed]
9. Choi, M.K.; Vu, C.C.; Kim, J.Y. Effects of Fe staple-fiber spun-yarns and correlation models on textile pressure sensors. *Sensors* **2022**, *22*, 3152. [CrossRef] [PubMed]
10. Hwang, Y.T.; Lee, S.H.; Lin, B.S. Assessment system for predicting maximal safe range for heel height by using force-sensing resistor sensors and regression models. *Sensors* **2022**, *22*, 3442. [CrossRef] [PubMed]
11. Junior, A.L.; Biazi, V.; Marques, C.; Frizera, A. Force-displacement analysis in diaphragm-embedded fiber Bragg grating sensors. *Sensors* **2022**, *22*, 5355. [CrossRef] [PubMed]
12. Yue, W.; Qi, J.; Song, X.; Fan, S.; Fortino, G.; Chen, C.H.; Xu, C.; Ren, H. Origami-inspired structure with pneumatic-induced variable stiffness for multi-DOF force-sensing. *Sensors* **2022**, *22*, 5370. [CrossRef] [PubMed]
13. Ministry of Land, Infrastructure and Transport. *Korean Railway Standards TR 0014-15R*; Ministry of Land, Infrastructure and Transport: Seoul, Republic of Korea, 2009.
14. Ansys Inc. *ANSYS®2007 ANSYS Workbench 2023 R1*; ANSYS Inc.: Cannonsberg, PA, USA, 2023.

Disclaimer/Publisher's Note: The statements, opinions and data contained in all publications are solely those of the individual author(s) and contributor(s) and not of MDPI and/or the editor(s). MDPI and/or the editor(s) disclaim responsibility for any injury to people or property resulting from any ideas, methods, instructions or products referred to in the content.